But Mouse, you are not alone: On some severe acute respiratory syndrome coronavirus 2 variants infecting mice

Michael J. Kuiper, PhD, is a Biomolecular Modeller who leads the Modelling and Simulations Team in at the CSIRO Data61, Dockands, Victoria, Australia

Laurence OW Wilson, PhD, is a Research Scientist who leads the Digital Genome Engineering Team at the CSIRO Transformational Bioinformatics Group, North Ryde, New South Wales, Australia

Shruthi Mangalaganesh, is studying Bachelor of Biomedical Science and Bachelor of Commerce at Monash University, Clayton, Victoria, Australia, and pursued an internship at the CSIRO Australian Centre for Disease Preparedness, Geelong, Victoria, Australia

Daniel Reti, BE(Hons), BS, worked as a Research Technician at the CSIRO Transformational Bioinformatics Group, North Ryde, New South Wales, Australia, and is currently Front-End Software Engineer at the Centre for Population Genomics, joint initiative of the Garvan Institute of Medical Research, Sydney, New South Wales, Australia and the Murdoch Children's Research Institute, Melbourne, Victoria, Australia

Seshadri S Vasan, DPhil, is a Senior Principal Research Consultant and COVID-19 Project Leader at the CSIRO Australian Centre for Disease Preparedness, Geelong, Victoria, Australia, and Honorary Professor in the Department of Health Sciences at the University of York, York, UK

Address correspondence to Professor Seshadri S Vasan, CSIRO Australian Centre for Disease Preparedness, 5 Portarlington Road, Geelong, 3220, Victoria, Australia or email vasan.vasan@csiro.au

NB: MJK and LOWW contributed equally to this paper.

Running Title: On some SARS-CoV-2 variants infecting mice

Abstract

In silico predictions combined with *in vitro*, *in vivo* and *in situ* observations collectively suggest that mouse adaptation of the SARS-CoV-2 virus requires an aromatic substitution in position 501 or position 498 (but not both) of the spike protein's receptor binding domain. This effect could be enhanced by mutations in positions 417, 484 and 493 (especially K417N, E484K, Q493K and Q493R), and to a lesser extent by mutations in positions 486 and 499 (such as F486L and P499T). Such enhancements due to more favourable binding interactions with residues on the complementary angiotensin-converting enzyme 2 (ACE2) interface, are however, unlikely to sustain mouse infectivity on their own based on theoretical and experimental evidence to date. Our current understanding thus points to the Alpha, Beta and Gamma

variants of concern infecting mice, while Delta and 'Delta Plus' lack a similar biomolecular basis to do so. This paper identifies a list of countries where local field surveillance of mice is encouraged because they may have come in contact with humans who had the virus with adaptive mutation(s). It also provides a systematic methodology to analyze the potential for other animal reservoirs and their likely locations.

Keywords

AlphaFold; animal reservoir; COVID-19; *in silico*; *in vitro*; *in vivo*; mouse adaptation; SARS-CoV-2; variants

Introduction

The 'novel coronavirus disease' (COVID-19) has resulted in significant global morbidity and mortality on a scale similar to the influenza pandemic of 1918.[1] The ongoing pandemic has been sustained through the activities of human beings, who are the largest reservoir of the causative 'severe acute respiratory syndrome virus 2' (SARS-CoV-2). This RNA virus in a new host (human beings) is evolving rapidly, accumulating mutations, and existing as a cloud of variants with quasispecies diversity.[2] Last year, the world witnessed the risk of this virus acquiring additional reservoirs (such as minks) and new mutations of consequence (such as 'Cluster 5'), which could increase transmissibility and lead to a potentially weaker antibody response.[3]

Both the original form of the virus (known as 'D614') and the subsequent more transmissible 'G614' variant which has replaced it almost entirely in circulation,[4,5] did not infect mice because their 'angiotensin-converting enzyme 2' (ACE2) receptor did not bind the viral spike protein effectively to allow entry into cells. Since mouse (*Mus musculus*) is a popular animal model of infection, the virus had to be adapted through techniques such as sequential passaging in mouse lung tissues and modifying the receptor binding domain (RBD).[6-8] Other strategies to infecting mice with the original form of the virus or

the G614 included transgenic mice expressing human ACE2 (hACE2), and sensitizing the mouse respiratory tract through transduction with adenovirus or adeno-associated virus expressing hACE2.[9-12] Recently, virus 'variants of concern' (VOC) originating from Brazil, South Africa and the UK (which contain the common mutation N501Y in the RBD) were shown to infect mice.[13,14] This ability of SARS-CoV-2 variants of concern to infect mice is unsettling because of the potential to establish additional reservoirs in a species that is in close contact with people and companion animals, especially as its population is hard to vaccinate or control.

Methodology

In this paper, we have combined our structural predictions from biomolecular modelling with available experimental evidence to understand how specific mutations in VOC and mouse adapted strains, especially in the RBD, have enabled this virus to infect mice. To do this, we compared interactions of these key mutations with the corresponding regions in both mouse ACE2 (mACE2) and hACE2 using molecular models based on crystallographic data of the ACE2/RBD interface (protein database 'pdb' entry number 6M17)[15]. As the improved protein prediction software *Alphafold* has just been made available, we used these new artificial intelligence methods to further validate our model structures.[16] By introducing the ACE2 models and variants into molecular dynamics simulations, similar to our recent work,[17,18] we qualitatively identified the key interactions of side chain residues at the ACE2/RBD interface. Further details are provided under Supplementary Methods for Molecular Modelling. We then compared our *in-silico* findings with experimental results reported by different research groups with mouse adapted strains/isolates[6-8,13,21-29] and VOC[14,30-34] (**Table 1**). Taken together, we were able to gain valuable insights into the likely effects of different mutations of consequence.

We then queried the world's largest public database called 'GISAID' (Global Initiative on Sharing All Influenza Data) and looked for these mutations, and equivalent mutations of consequence, in the circa 2.4 million SARS-CoV-2 genome sequences available as of 21 June 2021.[29] In brief, sequences were aligned to the back to the SARS-CoV-2 reference (EPI_ISL_402124, denoted as the WT allele) in order to generate a file containing all mutations in the variant call format (VCF), which is a concise way for storing gene sequence variations. We then calculated the ratio of the frequency at which the WT allele versus the mutant allele were observed across a rolling 14-day window. Given the data is discrete, highly variable in size across countries, and contains background noise, such a window of time is essential from our experience to reduce distortions and glean meaningful insights. For example, if 14 WT and 28 mutant sequences were observed within a specified 14-day window, then the frequencies were 1/day and 2/day respectively. The ratio of mutant:WT frequency is therefore 2, indicating the mutant allele is appearing twice as frequently as the WT allele within that period. This was used to create a heatmap for the key mutations, both individually and in combination (as discussed below). For clarity, we only considered countries where the mutant:WT ratio exceeded 1.2 across the entire time the mutant was sampled or within any given 14-day window. To reduce the noise further from low-sampled countries, we also instituted a minimum threshold of 10 WT and 10 mutant samples over at least 14 days to suggest possible spread locally. For this reason, a country where a mutant had only been recorded on a single day, or where only 9 mutant samples were recorded overall, was not included in our analysis. Our heatmap scale has also been truncated at 2.00 for ease of visual comparison.

Results and Discussion

In silico results

In silico comparison of the interface residues of the RBD/ACE2 complex in human and mouse models reveals 30 ACE2 residues in close contact, of which 19 are conserved between mACE2 and hACE2

(approximately 63% identity for the contacting ACE2 residues). The RBD mutations associated with the mouse adaptations listed in **Table 1** can be grouped loosely into 3 regions by their positions on the ACE2/RBD interface as follows: Region 1 (RBD positions 498, 499 and 501) are centered around the highly conserved ACE2 residue tyrosine 41 (Y41); Region 2 (RBD positions 417, 493) centered around ACE2 residue 34; and Region 3 (RBD positions 484 and 486) close to a cluster of ACE2 residues 78 to 82. ACE2 residues within 5 Å (chosen to account for molecular fluctuations) of each RBD adaptation are listed in **Table 2**, with dissimilar human/mouse ACE2 residues highlighted in yellow. **Figure 1** further illustrates these residues visually, and how they are relatively positioned in three regions. **Figure 2** aligns the human and mouse ACE2 to highlight the key differences at the contact points with the RDB (shown in yellow).

Modelling the N501Y mutation at the ACE2/RBD interface reveals a close interaction with the highly conserved Y41 residue in ACE2, through attractive, non-covalent bonding between aromatic amino acids known as π-stacking interactions. In mACE2, π-stacking can be enhanced by the proximal substitution of histidine (H) in place of lysine (K) which is present at position 353 of hACE2. Our modelling also shows similar π-stacking enhancement with the conserved Y41, through the substitution of RBD glutamine at position 498 (Q498) to either histidine (H) or tyrosine (Y). These aromatic π-stacking interactions appear to be reasonably strong as N501Y and Q498H can each sustain mouse adaptation on its own in experiments.[6,13,23,28] Counterintuitively, our modelling predicts that simultaneous aromatic mutations at RBD positions 498 and 501 is detrimental to mouse adaptation due to local π-stacking distortion to the binding interface. This could explain why we have not observed simultaneous aromatic mutations at these positions in over 2.4 million entries on GISAID as of 21 July 2021. We did detect one adapted isolate on GISAID from mouse lung homogenate where N501Y occurs with glutamate 498 to arginine (Q498R),[29] which strictly speaking is not aromatic, however arginine is frequently associated with π-stacking

interactions.[37] Thus, the Q498R mutation is more tolerated with N501Y due to arginine's inherent conformational flexibility compared to tyrosine or histidine.

In Region 1 (**Table 2**) we also note the proline 499 to threonine (P499T) substitution in two infectious clones, presumably engineered to enhance Y498. Modelling provides the following insight on this: the change from P to T will relax the backbone constraints of proline and allow conformational rearrangement of threonine to contact the conserved ACE2 residues Y41 and L45. However, we don't find any strong molecular modelling basis for this mutation to sustain mouse adaptation on its own or evolve naturally alongside adaptive mutations at positions 498 or 501; this is borne out by experimental evidence to date. In other words, *in silico* predictions combined with *in vitro* and *in vivo* evidence collectively suggest that mouse adaptation requires an aromatic substitution in either position 501 or position 498 (but not both); while additional mutations, especially in Region 2 and Region 3 of the RBD as summarized below, enhancing ACE2 binding interactions and specificity in mice. These predictions are further supported by *AlphaFold* that assigns very high confidence scores (>93 in a scale of 0-100) for the structural predictions involving these key mutations, demonstrating the applications of this improved protein prediction software especially during pandemics such as COVID-19 and future 'Disease-X'.

From **Table 1**, we see that mouse adapted strains sometimes carry the Q493K/R mutation (polar glutamine to basic lysine or arginine). Modelling predicts this as being enabled through favourable salt-bridge interactions with both glutamic acid 35 (E35) or aspartic acid 38 (D38) both of which are conserved in hACE2 as well as mACE2 (c.f. **Table 2**, Region 2). The K417N substitution (lysine to asparagine), which is another experimental observation from **Table 1**, is also predicted by modelling to be advantageous for mouse adaptation due to favourable amide hydrogen bond interactions with interfacial mACE2 residues asparagine 31 (N31) and glutamine 34 (Q34); such amide hydrogen bonding is not possible in hACE2 as it

has non-amide lysine (K) and histidine (H) residues. With the Gamma variant of concern, it is unclear whether the K417T enhances the role of N501Y in mouse adaptation in a similar manner. The 'Delta Plus' variant of concern has the K417N mutation, but there is no molecular modelling basis to believe that it can infect mice without an aromatic change in position 498 or 501 as described above. It would be worthwhile to further investigate any interfering role of glycosylation at this interface region, because hACE2 contains N-linked glycosylation at asparagine 90 (N90) whereas mACE2 does not (its analogous residue is threonine T90 according to Uniprot references Q8R0I0 and Q9BYF1).

In Region 3, the K484 residue is not positioned directly at the interface and not observed to interact strongly with any ACE2 residues; however, our model shows occasional salt bridges can be formed with relatively close glutamic acid residues in positions 35 and 75 that are conserved in both hACE2 and mACE2. Our simulations show that the distance between K484 and these glutamic acid residues fluctuate dynamically from 3 to 20 Å, with salt bridges more likely when distances are around 3 Å. Thus, the E484K, which is present in the Beta and Gamma variants of concern, and more recently in some Alpha isolates as well, is likely to have an enhancing role through transient salt bridges. The same cannot be said about E484Q seen in the Delta variant of concern because salt bridge formation is unlikely with the polar glutamine (Q) residue. With no accompanying aromatic change in positions 498 or 501, we believe that the E484Q in Delta, and additionally the K417N in 'Delta Plus', cannot sustain mouse infectivity on their own based on current biomolecular understanding. The residues 75 to 82 in mACE2 are significantly different from hACE2 (**Table 2**), therefore any mutation in the corresponding RBD interface is worth investigation. We could find one from experimental observations, the engineered substitution F486L,[27] and consider it to have at best an enhancing role. As it was observed simultaneously with Q498Y (which is likely to sustain mouse infectivity on its own), the contribution of F486L to the overall mouse adaptation remains to be ascertained.

Comparison with *in vitro*, *in vivo* and *in situ* observations

Early *in silico* predictions based on comparative structural analysis of ACE2 suggested that mouse has a very low probability of being infected.[35,36] Although correct about mouse, those analyses also made inconsistent and erroneous predictions that ferrets wouldn't be susceptible, pigs would be susceptible, etc., thus exposing the need for experimental inputs into the model. Therefore, this paper takes into account a range of experimental observations to cross-check our *in silico* predictions through biomolecular modelling. Wan *et al.* reasoned that "*mouse or rat ACE2 contains a histidine at the 353 position which does not fit into the virus-receptor interaction as well as a lysine does*". [35] While this is true of the original Wuhan strain containing asparagine 501 (N501) in the RBD, our modelling indicates why the tyrosine 501 mutation enables mouse infectivity, even on its own. In hACE2, lysine 353 (K353) creates a salt bridge with conserved aspartic acid 38 (D38). In mACE2, lysine 353 is replaced by the aromatic histidine (H353) to complete the salt bridge, as well as contribute to π-stacking with Y501 variant. The N501Y mutation will also lead to favorable π-stacking with the highly conserved tyrosine 41 (Y41) residue in mammalian ACE2, as suggested by Starr *et al*.[38] with deep scanning of RBD mutations and hACE2 affinity assays. These authors highlighted enhanced affinity of F501 (as it had the highest score), followed by Y501, V501, W501 and T501, in that order. But Y501 and T501 require only a single nucleotide change and have been observed more frequently *in situ* (**Figures 3a,3b**) – compared to F501, V501 and W501 which require 2, 2 and 3 nucleotide changes respectively. It is unsurprising that the latter variants requiring two or more changes were rarely observed *in situ* regardless of their high *in vitro* affinity scores from Starr *et al*.[38]

From the above and **Table 3**, we see that *in silico* analysis can provide valuable insights to interpret and bridge *in vitro*, *in vivo* and *in situ* observations on the RBD position 501. A similar analysis is possible with the alternative essential mutation for mouse adaptation at RBD position 498, where the *in vitro* affinity

enhancement order is H498, Y498, F498 and W498 according to Starr *et al*.[38] Of these, H498 (on its own) and Y498 (with enhancing RBD mutations) have been shown to result in mouse adaptation *in vivo* (**Table 1**);[7,8,23-28] Q498R was also reported once, unusually in combination with N501Y, isolated from mouse lung after 30 passages. However, *in situ* observations of these variants have been limited to R498 (15 occurrences) and H498 (3 occurrences) so far. It is clear from *in vitro*, *in vivo* and *in situ* analyses (**Table 3**) that H498, R498 and Y498 are possible but not yet common. This is consistent with our *in silico* predictions because H498 and Y498 are aromatic (enabling π-stacking with ACE2 Y41; similar to Y501), while R498 has conformational flexibility and can still be associated with π-stacking interactions.[37] H498 and R498 observed *in situ* require a single nucleotide change from Q498, while Y498 requires two nucleotide changes (or one change from H498).

Similar insights are also possible for the enhancing RBD mutations (c.f. **Table 1** and **Table 3**). From *in vivo* and *in situ* observations, we see that K417M is less common than K417N or K417T (**Figure 4a,4b**), although *in vitro* studies did not predict any enhancement.[38] *In silico* predictions show that all these require a single nucleotide change, but that N417 (and Q417) would benefit from amide hydrogen bonding. E484K is present in Beta and Gamma, and increasingly in Alpha VOC, while E484Q is present in the Kappa variant of interest that is related to the Delta VOC. In comparison to these two substitutions and notwithstanding higher *in vitro* affinity scores, R484 and T484 are infrequently observed *in situ*, which is consistent with our *in silico* predictions because they each require 2 nucleotide changes from E484, or one change from K484. The F486L and P499T were originally engineered *in vivo*, but have had sporadic *in situ* presence in human populations. *In silico* predictions suggest that the F486L mutation (accessible by three possible ways of a single nucleotide change) can aid mACE2 adaptation, due to the human-mouse differences in ACE2 at the 78-82 region; the P499T is also a single nucleotide change (but only one way from P to T) and predicted to be rare in comparison. Finally, *in silico* predictions for Q493 substituted by K, L or R (each a

single nucleotide change) are borne out *in vivo* and *in situ*, although their affinity scores from *in vitro* experiments are low. The affinity scores from Starr *et al*.[38] were developed for hACE2 (not mACE2), so we expected a greater correlation than what has been observed *in situ* in human populations, but perhaps it is still early in the pandemic to assess this definitively.

Some mutations in the essential as well as enhancing positions can lead to other mutations. For example, N501Y, the key mutation common to the Alpha, Beta, and Gamma variants of concern, can lead to F501 with a further nucleotide change. Similarly, the enhancing E484K mutation can also lead to R484 or T484 with a further nucleotide change. We examined whether *in situ* observations are consistent or contrary to our *in silico* predictions. Indeed, F501 was observed once in Germany (25 May 2021) and Mexico (22 June 2021), while the Y501 has been observed in these countries since 22 October 2020 and 31 January 2021 respectively. UK reported E484R in August 2020, followed by USA, Angola, Brazil and South Korea in February, April, May and June 2021 respectively. In each case, the E484K was detected prior to E484R – the former mutation circulating in UK, USA, Angola, Brazil and South Korea from April, March, August, April and December 2020 respectively. Similarly, E484T was only recently detected in the USA in June 2021, 15 months after the first report of E484K in that country. All eight instances are thus consistent with our prediction – whether this link is causal or a coincidence is worthy of investigation with local epidemiological data. While bioinformatics tools can provide useful insights, out of 78 COVID-positive cases only one sample is on average sent for virus genome sequencing, with huge variations across time and locations, and lots of missing meta-data.[39,40] This means we are more confident about ruling in (e.g. when a variant has been detected in a location) than ruling out the possibility of a mutation circulating purely based on *in silico* data, even if the latter is statistically large (2.4 million as of 21 June 2021).

Our analysis is not just of theoretical interest; it has huge practical applications because mice can be kept as pets, or come into contact with other pets like cats which are known to be susceptible. Also, mouse plague can occur in area of COVID-19 outbreaks or endemicity, as is currently the case in New South Wales and adjacent states of Australia.[41] In order to help public health and animal health professionals, **Figure 5a,5b** shows the countries where key essential and enhancing mutations listed in **Tables 1 and 3** (viz. N501Y, E484K and K417N/T) have co-occurred. **Supplementary Table S1** gives the raw data, down to regional counts for these combinations. We believe that this information will help locate areas at risk for appropriate mitigation measures.

Conclusion and further analyses

Assessing the risk of viruses adapting to new hosts requires careful interpretation of all available data from *in silico*, *in vivo*, *in vitro* and *in situ* sources. Understanding host adaptation at a molecular level, via modelling helps reconcile seemingly conflicting, experimental, and clinical observations while a pandemic is still in progress. We have demonstrated this with the SARS-CoV-2 virus adapting to mice. Our conclusions come with humility, as they are based on best available evidence up to this point, but allowing us and others to refine when more evidence becomes available. Armed with our collective understanding from different approaches, and bolstered by bioinformatics and emerging artificial intelligence technologies such as *AlphaFold*, we have shown how to position ourselves better to predict and mitigate virus host adaptations, not just for this pandemic but also for future Disease-X. Further analyses pertaining to COVID-19 should focus on the role of mutations beyond the spike and RBD; and explore other hosts like rats and other potential reservoir species (even those that previously exhibited low receptor activities[35,36,42]) which will be hard to vaccinate or control.

Supplementary Methods for Molecular Modelling

272 Molecular simulations were performed using NAMD2.14[43] with CHARM36m[44] forcefield employing a
273 'TIP3' water model. The SARS-CoV-2 spike/ACE2 model was a homology model based on the pdb structure
274 6M17.[15] Models consisted of the SARS-CoV-2 spike RBD domain (residues 330 to 530), while the truncated
275 mACE2 protein consisted of residues 19 to 600 built using Swiss Modeller.[45] Glycosylation of the spike and
276 mACE2 protein was manually constructed using Visual Molecular Dynamics (VMD). Simulations were
277 run with Periodic Boundary Conditions 'PBCs' using the 'NPT' isothermal-isobaric ensemble at
278 310K and 1 bar pressure employing Langevin dynamics. The PBCs were constant in the XY
279 dimensions. Long-range Coulomb forces were computed with the Particle Mesh Ewald method
280 with a grid spacing of 1 Å. 2 fs timesteps were used with non-bonded interactions calculated
281 every 2 fs and full electrostatics every 4 fs while hydrogens were constrained with the 'SHAKE'
282 algorithm. The cut-off distance was 12 Å with a switching distance of 10 Å and a pair-list distance
283 of 14 Å. Pressure was controlled to 1 atmosphere using the Nosé-Hoover Langevin piston method
284 employing a piston period of 100 fs and a piston decay of 50 fs. Trajectory frames were captured
285 every 100 ps. Variants were built from the main RBD/mouse ACE2 model by mutating residues to cover
286 the main mouse adaptation mutations listed in **Tables 1 and 3**. Models were simulated for 300
287 nanoseconds. Trajectories were visualized with VMD and Nanome.
288

289 **Acknowledgements**

290 This work was supported by funding from the Australian government's Department of Finance, National
291 Health and Medical Research Council, and the CSIRO Future Science Platforms (Principal Investigator:
292 S.S.V.). We are grateful for support from our colleagues at the Australian Centre for Disease Preparedness
293 (https://www.grid.ac/institutes/grid.413322.5) (especially Simran Chahal, Trevor Drew and Alexander
294 McAuley) and the Transformational Bioinformatics Group (especially Denis Bauer, Yatish Jain, Brendan

Hosking and Aidan Tay). The title is from the poem '*To a Mouse: On Turning her up in her Nest, with the Plough, November 1785*' by Scotland's national poet Robert Burns, in which he says that the mouse is not alone in proving foresight may be vain as the best-laid schemes of mice and men go oft awry (*But, Mousie, thou art no thy-lane, In proving foresight may be vain: The best-laid schemes o' Mice an' Men Gang aft agley*).

Author contributions

Conceptualization, methodology, and funding acquisition, S.S.V.; *in silico* analysis, M.J.K.; *in vitro* analysis, M.J.K. and S.S.V.; *in vivo* analysis, S.M. and S.S.V.; *in situ* analysis, L.O.W.W. and D.R.; writing – original draft preparation, S.S.V, M.J.K. and S.M.; writing – review and editing, all authors.

References

1. Dong E, Du H, Gardern L. An interactive web-based dashboard to track COVID-19 in real time. *Lancet Infectious Diseases.* 2020;20(5):533-534. Available at https://doi.org/10.1016/S1473-3099(20)30120-1 (accessed 1 December 2020).
2. Bauer DC, Tay AP, Wilson, LOW, et al. Supporting pandemic response using genomics and bioinformatics: A case study on the emergent SARS-CoV-2 outbreak. *Transboundary & Emerging Diseases*. 2020; 67(4):1453-1462. Available at https://doi.org/10.1111/tbed.13588 (accessed 1 December 2020).
3. Lassaunière R, Fonager J, Rasmussen, M, et al. Working paper on SARS-CoV-2 spike mutations arising in Danish mink, their spread to humans and neutralization data. 2020. Available at https://files.ssi.dk/Mink-cluster-5-short-report_AFO2 (accessed 1 December 2020).

4. Korber B, Fischer WM, Gnanakaran S, et al. Tracking changes in SARS-CoV-2 spike: Evidence that D614G increases infectivity of the COVID-19 virus. *Cell*. 2020; 182(4):812-827. Available at https://doi.org/10.1016/j.cell.2020.06.043 (accessed 1 December 2020).

5. Zhang J, Cai Y, Xiao T, et al. Structural impact on SARS-CoV-2 spike protein by D614G substitution. *Science*. 2021; 372(6541):525-530. Available at https://doi.org/10.1126/science.abf2303 (accessed 1 May 2021).

6. Gu H, Chen Q, Yang G, et al. Adaptation of SARS-CoV-2 in BALB/c mice for testing vaccine efficacy. *Science*. 2020; 369(6511):1603-1607. Available at https://doi.org/10.1126/science.abc4730 and https://www.biorxiv.org/content/10.1101/2020.05.02.073411v1 (accessed 1 December 2020).

7. Dinnon KH, Leist SR, Schäfer A, et al. A mouse-adapted model of SARS-CoV-2 to test COVID-19 countermeasures. *Nature*. 2020; 586:560-566. Available at https://doi.org/10.1038/s41586-020-2708-8 (accessed 1 December 2020).

8. Leist SR, Dinnon KH, Schäfer A, et al. A mouse-adapted SARS-CoV-2 induces acute lung injury and mortality in standard laboratory mice. *Cell*. 2020; 183:1070-1085. Available at https://doi.org/10.1016/j.cell.2020.09.050 (accessed 1 December 2020).

9. Yuan L, Tang Q, Cheng T, Xia N. Animal models for emerging coronavirus: progress and new insights. *Emerging Microbes & Infections*. 2020; 9(1):949-961. Available at https://doi.org/10.1080/22221751.2020.1764871 (accessed 15 May 2021).

10. Muñoz-Fontela C, Dowling WE, Funnell SGP, et al. Animal models for COVID-19. *Nature.* 2020; 586: 509-515. Available at https://doi.org/10.1038/s41586-020-2787-6 (accessed 1 December 2020).

11. Zeiss CJ, Compton S, Veenhuis, RT. Animal models of COVID-19. I. Comparative virology and disease pathogenesis. *ILAR Journal*. 2021; ilab007. Available at https://doi.org/10.1093/ilar/ilab007 (accessed 1 May 2021).

12. Veenhuis RT, Zeiss CJ. Animal models of COVID-19 II. Comparative immunology. *ILAR Journal*. 2021; ilab010. Available at https://doi.org/10.1093/ilar/ilab010 (accessed 1 May 2021).

13. Rathnasinghe R, Jangra S, Cupic A, et al. The N501Y mutation in SARS-CoV-2 spike leads to morbidity in obese and aged mice and is neutralized by convalescent and post-vaccination human sera. *medRxiv.* 2021; 2021.01.19.21249592. Available at https://doi.org/10.1101/2021.01.19.21249592 (accessed 1 February 2021).

14. Yao W, Wang Y, Ma D, et al. Circulating SARS-CoV-2 variants B.1.1.7, 501Y.V2, and P.1 have gained ability to utilize rat and mouse Ace2 and altered in vitro sensitivity to neutralizing antibodies and ACE2-Ig. *bioRxiv*. 2021; 2021.01.27.428353. Available at https://doi.org/10.1101/2021.01.27.428353 (accessed 1 May 2021).

15. Yan R, Zhang Y, Li Y, et al. Structural basis for the recognition of SARS-CoV-2 by full-length human ACE2. *Science*. 2020; 367:1444-1448. Available at https://doi.org/10.1126/science.abb2762 (accessed 1 December 2020).

16. Jumper, J., Evans, R., Pritzel, A. *et al.* Highly accurate protein structure prediction with AlphaFold. *Nature* (2021). Available at https://doi.org/10.1038/s41586-021-03819-2 (accessed 20 July 2021).

17. McAuley AJ, Kuiper MJ, Durr PA, et al. Experimental and *in silico* evidence suggests vaccines are unlikely to be affected by D614G mutation in SARS-CoV-2 spike protein. *npj Vaccines*. 2020; 5:96. Available at https://doi.org/10.1038/s41541-020-00246-8 (accessed 1 December 2020).

361 18. Riddell S, Goldie S, McAuley A, et al. Live virus neutralisation of the 501Y.V1 and 501Y.V2 SARS-
362 CoV-2 variants following INO-4800 vaccination of ferrets. *bioRxiv*. 2021; 2021.04.17.440246.
363 Available at https://doi.org/10.1101/2021.04.17.440246 (accessed 1 May 2021).
364 19. Tai W, He L, Zhang X. Characterization of the receptor-binding domain (RBD) of 2019 novel
365 coronavirus: implication for development of RBD protein as a viral attachment inhibitor and
366 vaccine. Cellular & Molecular Immunology. 2020; 17:613-620. Available at
367 https://doi.org/10.1038/s41423-020-0400-4 (accessed 1 December 2020).
368 20. Grantham, R. Amino acid difference formula to help explain protein evolution. *Science*. 1974;
369 185(4154): 862-864. Available at https://doi.org/10.1126/science.185.4154.862 (accessed 1
370 December 2020).
371 21. Sun S, Gu H, Cao L, et al. Characterization and structural basis of a lethal mouse-adapted SARS-
372 CoV-2. bioRxiv. 2020; 2020.11.10.377333. Available at
373 https://doi.org/10.1101/2020.11.10.377333 (accessed 1 December 2020).
374 22. Fagre A, Lewis J, Eckley M, et al. SARS-CoV-2 infection, neuropathogenesis and transmission
375 among deer mice: Implications for spillback to New World rodents. *PLoS Pathogens*. 2021; 17(5):
376 e1009585. Available at https://doi.org/10.1371/journal.ppat.1009585 (accessed 24 May 2021).
377 23. Wang J, Shuai L, Wang C, et al. Mouse-adapted SARS-CoV-2 replicates efficiently in the upper
378 and lower respiratory tract of BALB/c and C57BL/6J mice. *Protein & Cell*. 2020; 11:776-782.
379 Available at https://doi.org/10.1007/s13238-020-00767-x (accessed 1 December 2020).
380 24. Liu Z, Zheng H, Lin H, et al. Identification of common deletions in the spike protein of Severe
381 Acute Respiratory Syndrome Coronavirus 2. *Journal of Virology.* 2020; 94(17):e00790-20.
382 Available at https://doi.org/10.1128/JVI.00790-20 (accessed 1 December 2020).
383 25. Zhou H, Chen X, Hu T, et al. A novel bat coronavirus closely related to SARS-CoV-2 contains
384 natural insertions at the S1/S2 cleavage site of the spike protein. *Current Biology.* 2020;

30:2196-2203. Available at https://doi.org/10.1016/j.cub.2020.05.023 (accessed 1 December 2020).

26. Huang K, Zhang Y, Hui X, et al. Q493K and Q498H substitutions in spike promote adaptation of SARS-CoV-2 in mice. *EBioMedicine*. 2021; 67:103381. Available at https://doi.org/10.1016/j.ebiom.2021.103381 (accessed 24 May 2021).

27. Muruato A, Vu MN, Johnson BA, et al. Mouse adapted SARS-CoV-2 protects animals from lethal SARS-CoV challenge. *bioRxiv.* 2021; 2021.05.03.442357. Available at https://doi.org/10.1101/2021.05.03.442357 (accessed 15 May 2021).

28. Zhang Y, Huang K, Wang T, et al. SARS-CoV-2 rapidly adapts in aged BALB/c mice and induces typical pneumonia. *Journal of Virology.* 2021; 95(11):e02477-20. Available at https://doi.org/10.1128/JVI.02477-20 (accessed 24 May 2021).

29. Van Noorden, R. Scientists call for fully open sharing of coronavirus genome data. *Nature*. 2021; 590:195-196. Available at https://doi.org/10.1038/d41586-021-00305-7 (accessed 1 March 2021).

30. Rambaut A, Loman N, Pybus O, et al. Preliminary genomic characterisation of an emergent SARS-CoV-2 lineage in the UK defined by a novel set of spike mutations. *Virological*. 2020. Available at https://virological.org/t/preliminary-genomic-characterisation-of-an-emergent-sars-cov-2-lineage-in-the-uk-defined-by-a-novel-set-of-spike-mutations/563 (accessed 1 March 2021).

31. Li Q, Nie J, Wu J, et al. SARS-CoV-2 501Y.V2 variants lack higher infectivity but do have immune escape. *Cell.* 2021; 184(9):2362-2371. Available at https://doi.org/10.1016/j.cell.2021.02.042 (accessed 1 May 2021).

32. Montagutelli X, Prot M, Levillayer L, et al. The B1.351 and P.1 variants extend SARS-CoV-2 host range to mice. *bioRxiv.* 2021; 2021.03.18.436013. Available at https://doi.org/10.1101/2021.03.18.436013 (accessed 1 May 2021).

33. Faria NR, Claro IM, Candido D, et al. Genomic characterisation of an emergent SARS-CoV-2 lineage in Manaus: preliminary findings. *Virological*. 2021. Available at https://virological.org/t/genomic-characterisation-of-an-emergent-sars-cov-2-lineage-in-manaus-preliminary-findings/586 (accessed 1 March 2021).

34. Lucaci AG, Zehr JD, Shank SD, et al. RASCL: Rapid assessment of SARS-COV-2 clades enabled through molecular sequence analysis and its application to B.1.617.1 and B.1.617.2. *Virological*. 2021. Available at https://virological.org/t/rascl-rapid-assessment-of-sars-cov-2-clades-enabled-through-molecular-sequence-analysis-and-its-application-to-b-1-617-1-and-b-1-617-2/709 (accessed 29 May 2021).

35. Wan Y, Shang J, Graham R, et al. Receptor recognition by novel coronavirus from Wuhan: an analysis based on decade-long structural studies of SARS coronavirus. *Journal of Virology.* 2020; 94(7):e00127-20. Available at https://doi.org/10.1128/JVI.00127-20 (accessed on 1 December 2020).

36. Damas J, Hughes GM, Keough C, et al. Broad host range of SARS-CoV-2 predicted by comparative and structural analysis of ACE2 in vertebrates. *PNAS.* 2020; 117(36):22311-22322. Available at https://doi.org/10.1073/pnas.2010146117 (accessed 1 December 2020).

37. Flocco MM, Mowbray SL. Planar stacking interactions of arginine and aromatic side-chains in proteins. *Journal of Molecular Biology*. 1994; 235(2):709-717. Available at https://doi.org/10.1006/jmbi.1994.1022 (accessed 1 December 2020).

38. Starr TN, Greaney AJ, Hilton SK, et al. Deep mutational scanning of SARS-CoV-2 receptor binding domain reveals constraints on folding and ACE2 binding. *Cell*. 2020; 182(5):1295-1310.e20. Available at https://doi.org/10.1016/j.cell.2020.08.012 (accessed 1 December 2020).

39. Bauer DC, Metke-Jimenez A, Maurer-Stroh S, et al. Interoperable medical data: the missing link for understanding COVID-19. *Transboundary & Emerging Diseases*. 2021; 68(4):1753-1760. Available at https://onlinelibrary.wiley.com/doi/10.1111/tbed.13892 (accessed 1 July 2021).

40. Priyadarshini, S. Massive coronavirus sequencing efforts urgently need patient data. *Nature India (special issue #13 on COVID-19 crisis)*. 2020; 10.1038/nindia.2020.75:11-13. Available at https://www.natureasia.com/en/nindia/pdf/special-issues/13/Nature-India-COVID-19-Crisis.pdf and https://go.nature.com/2y7kUIw (accessed 1 December 2020).

41. NSW Government. Help for regional communities impacted by the mouse plague. 2021. Available at https://www.nsw.gov.au/initiative/mouse-control-support-program (accessed 24 May 2021).

42. Zhao X, Chen D, Szabla R, et al. Broad and differential animal angiotensin-converting enzyme 2 receptor usage by SARS-CoV-2. *Journal of Virology*. 2020; 94(18):e00940-20. Available at https://doi.org/10.1128/JVI.00940-20 (accessed 1 December 2020).

43. Phillips JC, Braun R, Wang W, et al. Scalable molecular dynamics with NAMD. *Journal of Computational Chemistry*. 2005; 26:1781-1802. Available at https://doi.org/10.1002/jcc.20289 (accessed 1 December 2020).

44. Huang J, Rauscher S, Nawrocki G, et al. CHARMM36m: an improved force field for folded and intrinsically disordered proteins. *Nature Methods.* 2017; 14:71-73. Available at: https://doi:10.1038/nmeth.4067 (accessed 1 December 2020).

45. Waterhouse A, Bertoni M, Bienert S, et al. SWISS-MODEL: homology modelling of protein structures and complexes. *Nucleic Acids Research*. 2018; 46:W296-W303. Available at https://doi.org/10.1093/nar/gky427 (accessed 1 December 2020).

Mice-infecting SARS-CoV-2 'strains'/isolates	Key mutations in the spike RBD (residues 331-524)[19]							Color legend – mutations scored on Grantham Distance,[20] in the scale of 5 (conservative) to 215 (radical), similar to Riddell et al.[18]										
	K417	E484	F486	Q493	Q498	P499	N501	22	24	38	43	53	56	73	94	95	99	143
Mouse Adapted (MA) strains								**Authors' synthesis/comments**										
MASCp6[6]							N→Y	L37F (nsp6), P84S (nsp10), and D128Y (N) were the other observed nonsynonymous mutations.										
MASCp25[21]				Q→K			N→Y	MASCp6 passaged serially to develop MASCp25 and MASCp36, which accumulated Q493K and subsequently K417N in the RBD.										
MASCp36[21]	K→N			Q→K			N→Y	Highly virulent in aged mice and reported stable/mature RBD binding. It also had I1258V (nsp3), S301L (nsp5), and R32C (N).										
IC-MA1[7]					Q→Y	P→T		Spike Q498Y and P499T were engineered for compatibility with Q42 of mouse ACE2.										
IC-MA10[8]				Q→K	Q→Y	P→T		Q493K evolved in MA10 and interacts with mACE2's N31; others were T285I (nsp4), K2R (nsp7), E23G (nsp8), and F7S (ORF6).										
WA1-MA-P11[13]							N→Y	In addition to N501Y, there were H655Y, T7I (M), L84S (ORF8), S194T (N) and the +KLRS (216-219) insertion also observed by others and predicted to form a solvent-accessible loop.[22]										
HRB26M[23] (HRB26-P14)					Q→H			HRB26-P5 had Q498H, N969S, and the 675QTQTN679 deletion observed by others.[24,25] P14 also had A81T (nsp8).										
Hu-1-WBP-1[26]				Q→K	Q→H			Q493K and Q498H by P5, interacting respectively with mACE2's N31 via H-bond and Y41 via π-stacking. Nonsynonymous Q493K and T77I (nsp9) mutations increased frequency from P8 to P11.										
IC-MA4[27]			F→L		Q→Y			F486L and Q498Y were engineered for infecting mice.										
IC-CMA1-3[27]	K→N						N→Y	CMA1-3 all had N501Y. CMA2 also had D128Y; CMA3 also had D128Y, L37F, and P87S. Passaging of CMA3 resulted in K417N, H655Y, and E8V (E).										
LG[28]					Q→H			Other mutations present were N74K, H655Y, I6V (ORF10).										
IA-N501Y-MA30	K→M	E→K		Q→R	Q→R		N→Y	Homogenate from BALB/c mouse lung after 30 passages. GISAID entry EPI_ISL_1666328.[29]										
Variants of Concern (VOC) infecting mice																		
Alpha (501Y.V1 or B.1.1.7[14,30])		E→K					N→Y	First reported in the UK, September 2020. Spike also has A570D, P681H, T716I, S982A, and D1118H, in addition to HV69-70 and Y144 deletions. **E484K has been detected in this VOC in 15 countries as of 29 April 2021 (436 entries on GISAID).**										
Beta (501Y.V2 or B.1.351[14,31,32])	K→N	E→K					N→Y	First reported in South Africa, May 2020. V2-1 had D80A, D215G, E484K, N501Y, D614G and A701V in the Spike. L18F and K417N arose in V2-2. V2-3 had 242-244 deletion.										
Gamma (501Y.V3 or P.1[14,32,33])	K→T	E→K					N→Y	First reported in Brazil, November 2020. L18F, T20N, P26S, D138Y, R190S, K417T, E484K, N501Y, H655Y and T1027I in Spike.										
VOC not known to infect mice																		
Delta (452R.V3 or B.1.617.2)[34]	K→N							First reported in India, October 2020. Also has L452R in the RBD; G142D, R158G, T478K, P681R and D950N in Spike, along with deletions 156-157. **K417N has been detected in this VOC (called 'Delta Plus') in 12 countries as of 25 June 2021.** The related Kappa variant of interest (B.1.617.1) has L452R and E484Q in RBD (Grantham Distance scores of 102 and 29 respectively).										

Table 1 Key mutations in 14 'mouse adapted strains' and 3 'variants of concern' of SARS-CoV-2 known to infect mice

	SARS-CoV-2 RBD mouse adaptations	human/mouse ACE2 interface residues within 5 Å of mutation
Region 1	**N501 Y**	38D/D, 41Y/Y, **353K/H**, 355D/D, 357R/R
	P499 T	41Y/Y, 45L/L, **329E/A**, 330N/N
	Q498 H/R/Y	41Y/Y, 42Q/Q, 45L/L, 49N/N, **61N/K**, 357R/R
Region 2	**Q493 K/R**	**34H/Q**, 35E/E, 38D/D, 42Q/Q
	K417 M/N/T	**31K/N**, **34H/Q**
Region 3	**E484 K/Q**	35E/E, 75E/E
	F486 L	75E/E, 76Q/Q, **78 T/K**, **79 L/T**, **82 M/S**

Table 2. SARS-CoV-2 spike RBD mutations associated with mouse adaptation and their close contact residues in respective ACE2 proteins. Positions with dissimilar human/mouse residues are highlighted in yellow.

	Essential position in RBD		Enhancing position(s) in RBD for mouse adaptation				
Analysis	Q498	N501	K417	E484	F486	Q493	P499
In silico [1]	H Y F W [5]	Y H F W [5]	N Q [8]	K Q	L	K L R	T
In vitro [2]	H Y F W	F Y V W T	-	R K T Q	-	M A Y F K L V	-
In vivo [3]	H R Y	Y	M N T	K Q	L	K R	T
In situ [4]	R H [6]	Y T H F [7]	N T M [9]	K Q R T [10]	L [11]	K L R [12]	T [13]

1. Predicted by our modelling. For E484, F486, Q493, and P499 our work only reconfirmed *in vivo* observations.

2. Arranged in descending order of affinity binding from *in vitro* experiments reported by Starr *et al*.[38]

3. Observed *in vivo* with studies summarized in Table 1 (alphabetical order). Note L486 and P499 were engineered.

4. Observed on GISAID as of 21 July 2021 after removing noise from low sample countries. Only key trends are presented.

5. These aromatic residues are predicted to have similar interactions with Y41 of ACE2.

6. F W Y not observed yet. R (France, Germany, Netherlands) observed in mid 2021. H (Slovenia, USA) observed since early 2021.

7. V W not observed yet. H observed in Norway (early 2021) and F in Mexico (mid 2021). Y and T observed in several countries (**Figure 3a,b**).

8. Modelled mutations predict favorable amide hydrogen bonding. N and Q mutations each require a single nucleotide changes but there are 2 ways to get from N to K.

9. Q not observed yet. N (mutation G22813T) and T observed several countries (**Figure 4a,b**). Interestingly, N (alternative mutation G22813C) has sporadic presence in UK and USA (since late 2020).

10. K and Q observed in several countries (Figures 7,8). Sporadic presence of T (USA in mid 2021), and R (Angola and South Korea since mid 2021) observed.

11. Sporadic presence of different synonymous mutations (T23018C in Netherlands and Columbia; T23020G in USA) observed since late 2020.

12. A, F, M, V, Y not observed yet. Sporadic presence observed for K (Italy since early 2020), L (Trinidad and Tobago in mid 2021) and R (Czech Republic and Romania mid 2021).

13. Sporadic presence since late 2020 in Netherlands, Bulgaria and Canada.

Table 3 Comparison of *in silico*, *in vitro*, *in vivo* and *in situ* observations of key mutations in **Table 1**.

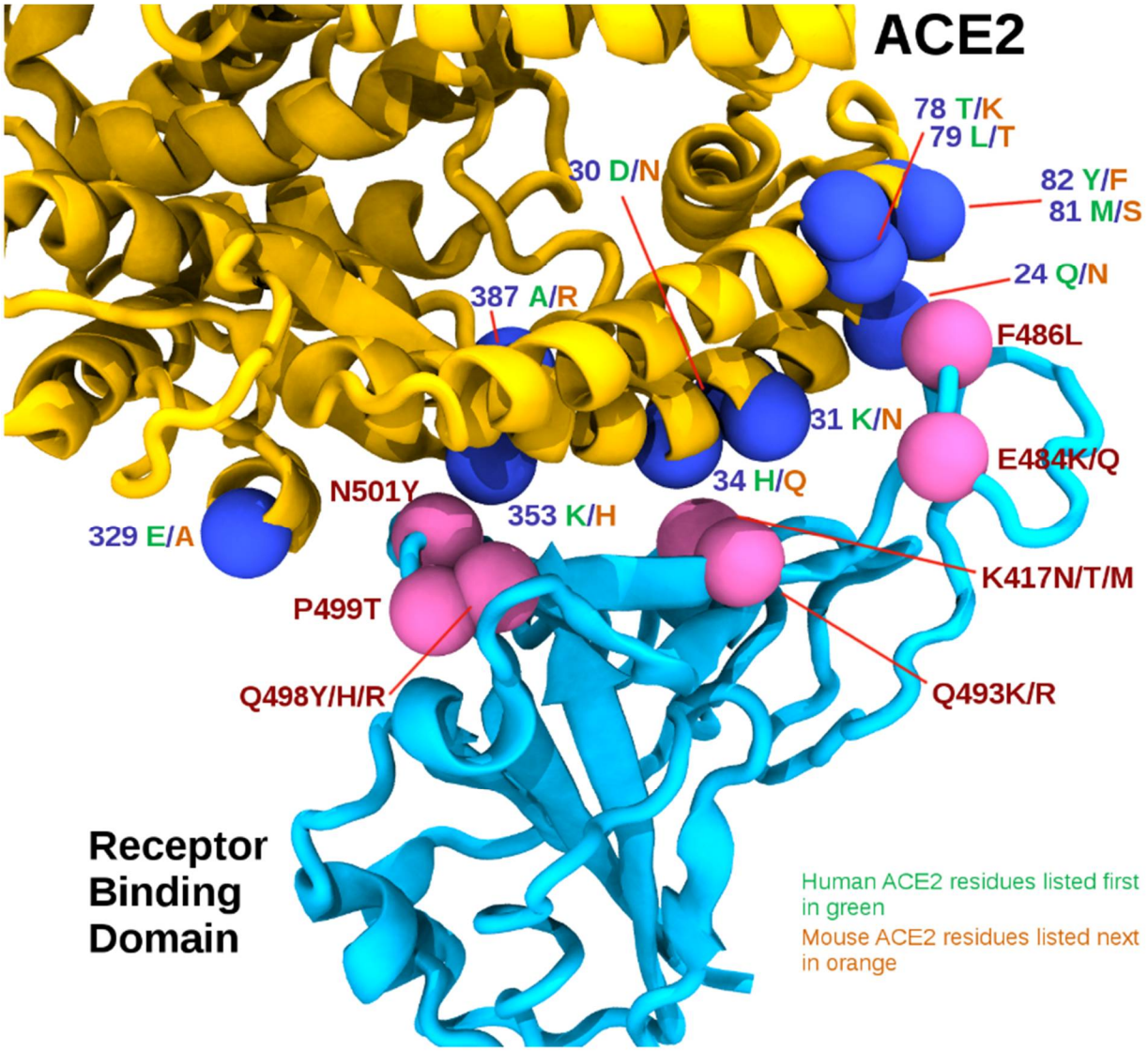

Figure 1. The RBD/ACE2 interface. The receptor binding domain (RBD) is shown in cyan, while the ACE2 is shown in yellow. Pink spheres indicate relative positions of mouse adapting mutations on the RBD, while the blue spheres represent interface residues that differ between human and mouse ACE2 sequences, shown in green and orange respectively.

```
SP|Q9BYF1|ACE2_HUMAN MSSSSWLLLS LVAVTAAQST IEEQAKTFLD KFNHEAEDLF YQSSLASWNY NTNITEENVQ 60
SP|Q8R0I0|ACE2_MOUSE MSSSSWLLLS LVAVTTAQSL TEENAKTFLN NFNQEAEDLS YQSSLASWNY NTNITEENAQ 60
                     ********** *****:***   **:******: :**:*****  ********** ********.*

SP|Q9BYF1|ACE2_HUMAN NMNNAGDKWS AFLKEQSTLA QMYPLQEIQN LTVKLQLQAL QQNGSSVLSE DKSKRLNTIL 120
SP|Q8R0I0|ACE2_MOUSE KMSEAAAKWS AFYEEQSKTA QSFSLQEIQT PIIKRQLQAL QQSGSSALSA DKNKQLNTIL 120
                     :*.:*. *** ** :***. * * : *****.   :* ***** **.***.**  **.*:*****

SP|Q9BYF1|ACE2_HUMAN NTMSTIYSTG KVCNPDNPQE CLLLEPGLNE IMANSLDYNE RLWAWESWRS EVGKQLRPLY 180
SP|Q8R0I0|ACE2_MOUSE NTMSTIYSTG KVCNPKNPQE CLLLEPGLDE IMATSTDYNS RLWAWEGWRA EVGKQLRPLY 180
                     ********** *****.**** ********:* ***.* ***. ******.**: **********

SP|Q9BYF1|ACE2_HUMAN EEYVVLKNEM ARANHYEDYG DYWRGDYEVN GVDGYDYSRG QLIEDVEHTF EEIKPLYEHL 240
SP|Q8R0I0|ACE2_MOUSE EEYVVLKNEM ARANNYNDYG DYWRGDYEAE GADGYNYNRN QLIEDVERTF AEIKPLYEHL 240
                     ********** ****:*:*** ********.: *.***:*.*. *******:**  *********

SP|Q9BYF1|ACE2_HUMAN HAYVRAKLMN AYPSYISPIG CLPAHLLGDM WGRFWTNLYS LTVPFGQKPN IDVTDAMVDQ 300
SP|Q8R0I0|ACE2_MOUSE HAYVRRKLMD TYPSYISPTG CLPAHLLGDM WGRFWTNLYP LTVPFAQKPN IDVTDAMMNQ 300
                     ***** ***: :******* * ********** *********  *****.**** *******::*
                                                |329                       |353
SP|Q9BYF1|ACE2_HUMAN AWDAQRIFKE AEKFFVSVGL PNMTQGFWEN SMLTDPGNVQ KAVCHPTAWD LGKGDFRILM 360
SP|Q8R0I0|ACE2_MOUSE GWDAERIFQE AEKFFVSVGL PHMTQGFWAN SMLTEPADGR KVVCHPTAWD LGHGDFRIKM 360
                     .***:***:* ********** *:******* * ****:*.: : *.******** **:***** *
                                                |387
SP|Q9BYF1|ACE2_HUMAN CTKVTMDDFL TAHHEMGHIQ YDMAYAAQPF LLRNGANEGF HEAVGEIMSL SAATPKHLKS 420
SP|Q8R0I0|ACE2_MOUSE CTKVTMDNFL TAHHEMGHIQ YDMAYARQPF LLRNGANEGF HEAVGEIMSL SAATPKHLKS 420
                     *******:** ********** ******* *** ********** ********** **********
```

Figure 2 Sequence alignment of human and mouse ACE2 highlighting contact points with the SARS-CoV-2 spike receptor binding domain in yellow. Differences between contact points are highlighted in green (human) and orange (mouse), while common contact residues are highlighted in cyan.

-

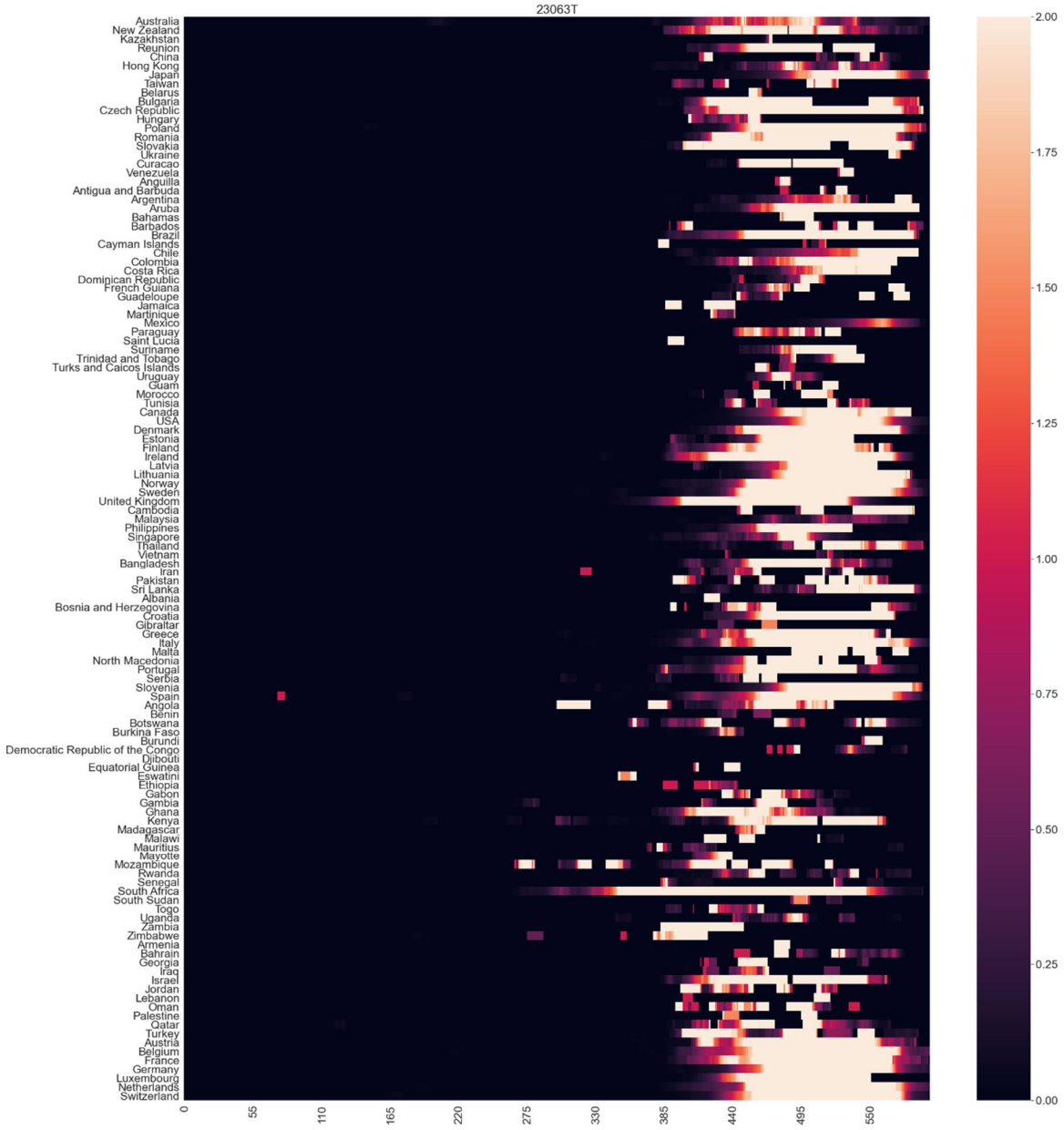
23063T
Australia
New Zealand
Kazakhstan
Reunion
China
Hong Kong
Japan
Taiwan
Belarus
Bulgaria
Czech Republic
Hungary
Poland
Romania
Slovakia
Ukraine
Curacao
Venezuela
Anguilla
Antigua and Barbuda
Argentina
Aruba
Bahamas
Barbados
Brazil
Cayman Islands
Chile
Colombia
Costa Rica
Dominican Republic
French Guiana
Guadeloupe
Jamaica
Martinique
Mexico
Paraguay
Saint Lucia
Suriname
Trinidad and Tobago
Turks and Caicos Islands
Uruguay
Guam
Morocco
Tunisia
Canada
USA
Denmark
Estonia
Finland
Ireland
Latvia
Lithuania
Norway
Sweden
United Kingdom
Cambodia
Malaysia
Philippines
Singapore
Thailand
Vietnam
Bangladesh
Iran
Pakistan
Sri Lanka
Albania
Bosnia and Herzegovina
Croatia
Gibraltar
Greece
Italy
Malta
North Macedonia
Portugal
Serbia
Slovenia
Spain
Angola
Benin
Botswana
Burkina Faso
Burundi
Democratic Republic of the Congo
Djibouti
Equatorial Guinea
Eswatini
Ethiopia
Gabon
Gambia
Ghana
Kenya
Madagascar
Malawi
Mauritius
Mayotte
Mozambique
Rwanda
Senegal
South Africa
South Sudan
Togo
Uganda
Zambia
Zimbabwe
Armenia
Bahrain
Georgia
Iraq
Israel
Jordan
Lebanon
Oman
Palestine
Qatar
Turkey
Austria
Belgium
France
Germany
Luxembourg
Netherlands
Switzerland
0
55
110
165
220
275
330
385
440
495
550
2.00
1.75
1.50
1.25
1.00
0.75
0.50
0.25
0.00

a)

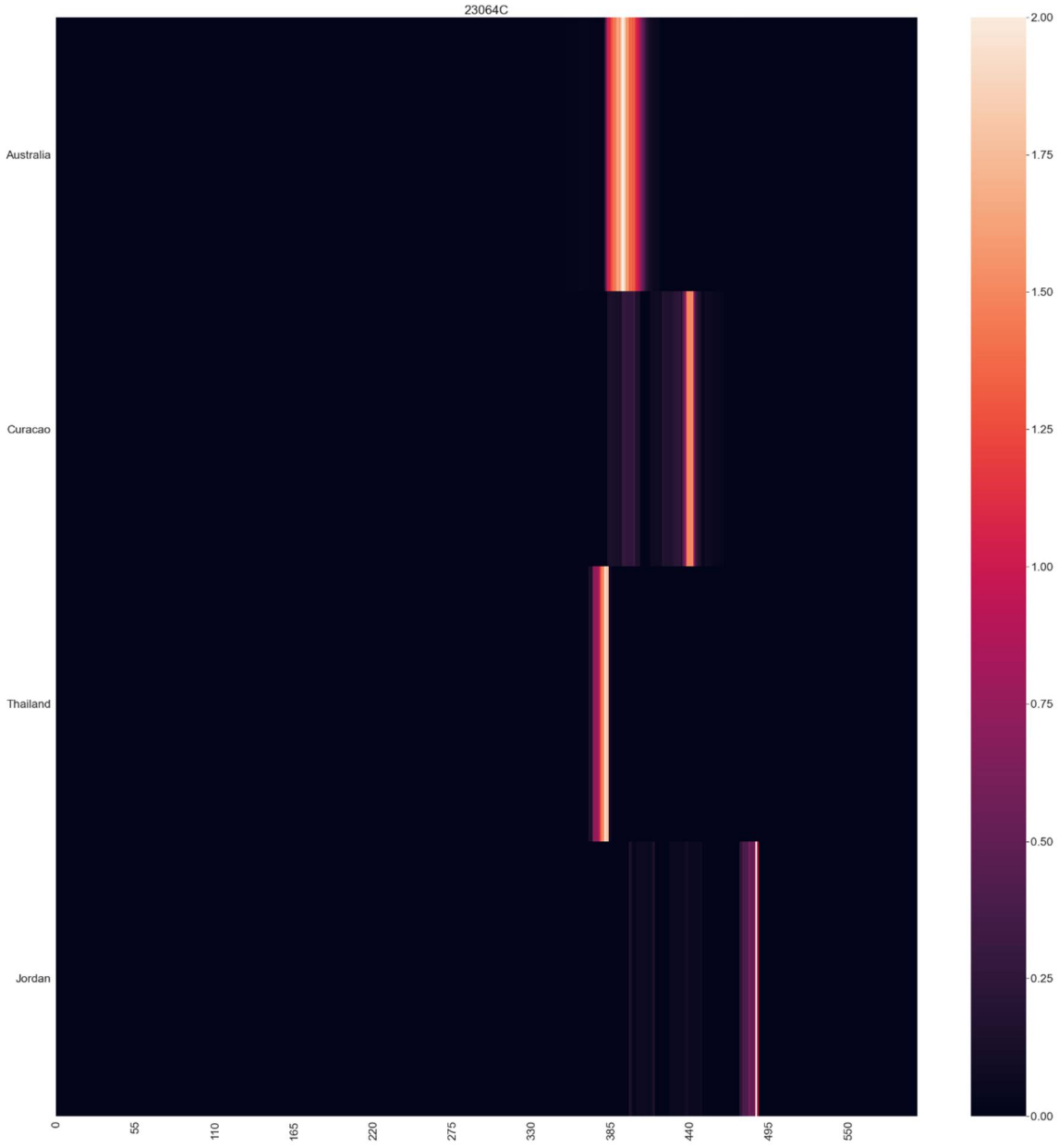

b)

Figure 3. Significant occurrences on GISAID of **a)** N501Y mutation (nucleotide change A23063T), and **b)** N501T mutation (nucleotide change A23064C), at the virus Receptor Binding Domain (RBD) since the start of the COVID-19 pandemic (31 December 2019).

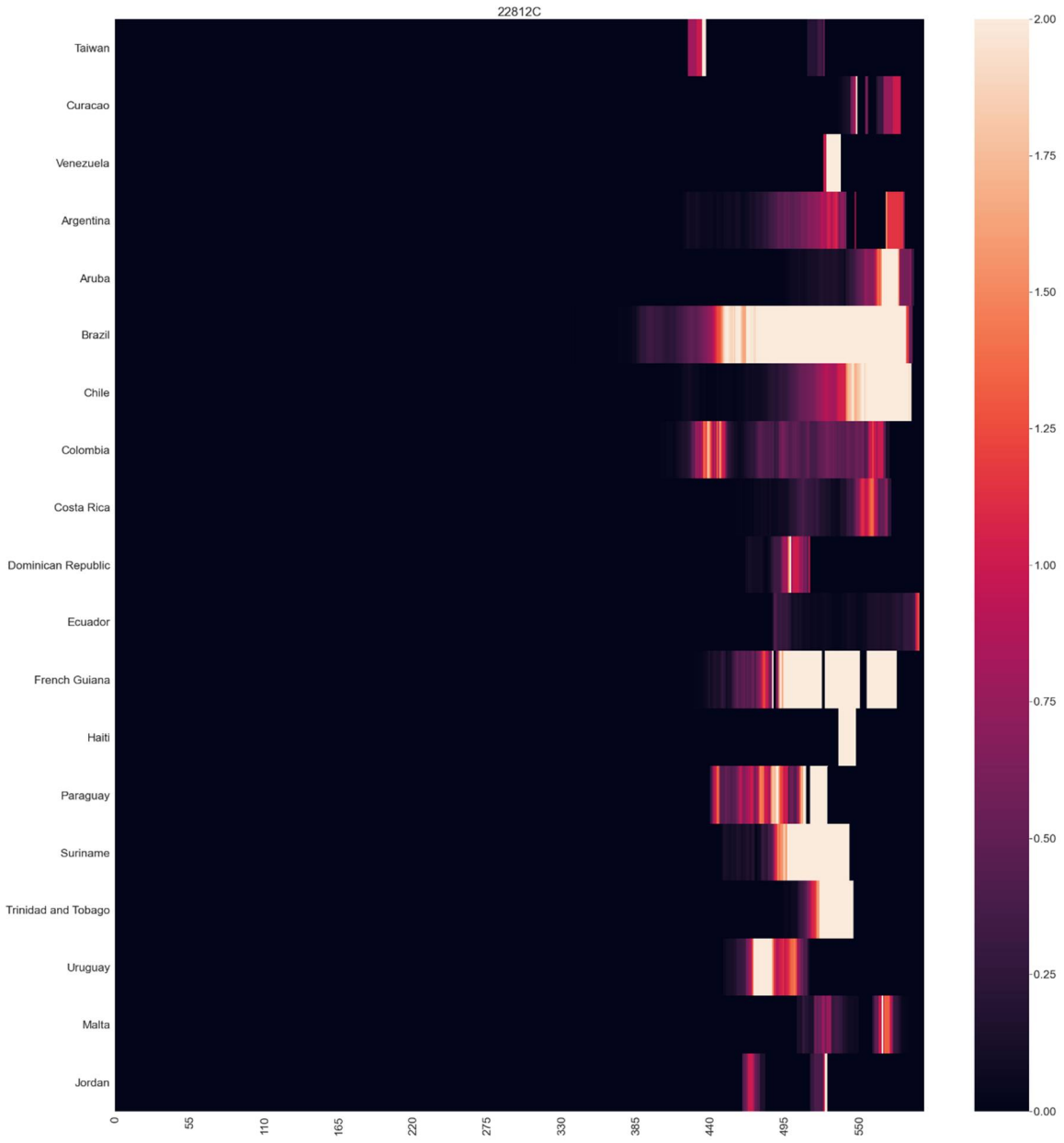
22812C
Taiwan
Curacao
Venezuela
Argentina
Aruba
Brazil
Chile
Colombia
Costa Rica
Dominican Republic
Ecuador
French Guiana
Haiti
Paraguay
Suriname
Trinidad and Tobago
Uruguay
Malta
Jordan
0
55
110
165
220
275
330
385
440
495
550
2.00
1.75
1.50
1.25
1.00
0.75
0.50
0.25
0.00

a)

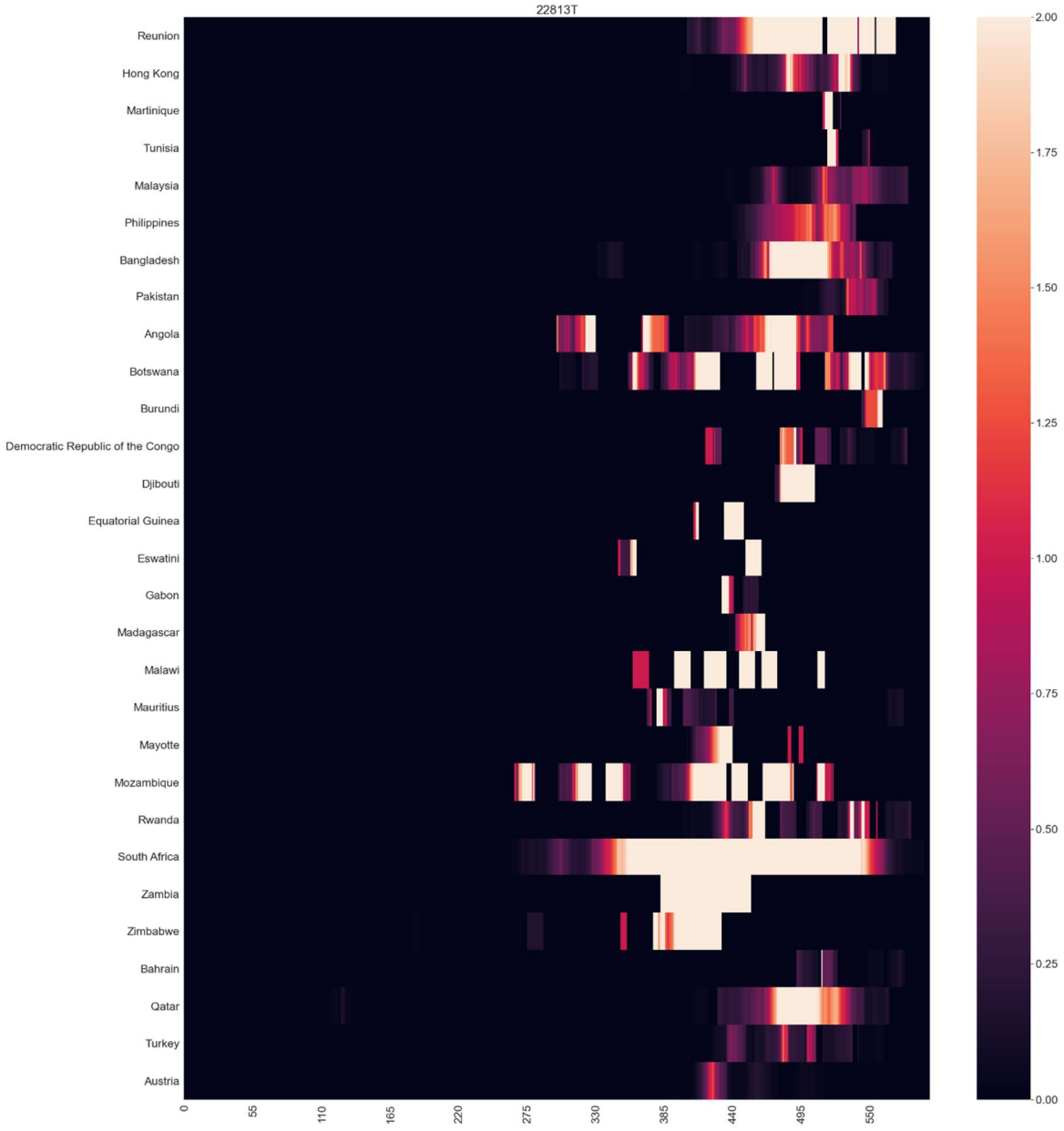

b)

Figure 4. Significant occurrences on GISAID of **a)** K417N mutation (nucleotide change G22813T), and **b)** K417T mutation (nucleotide change A22812C), at the virus Receptor Binding Domain (RBD), since the start of the COVID-19 pandemic (31 December 2019).

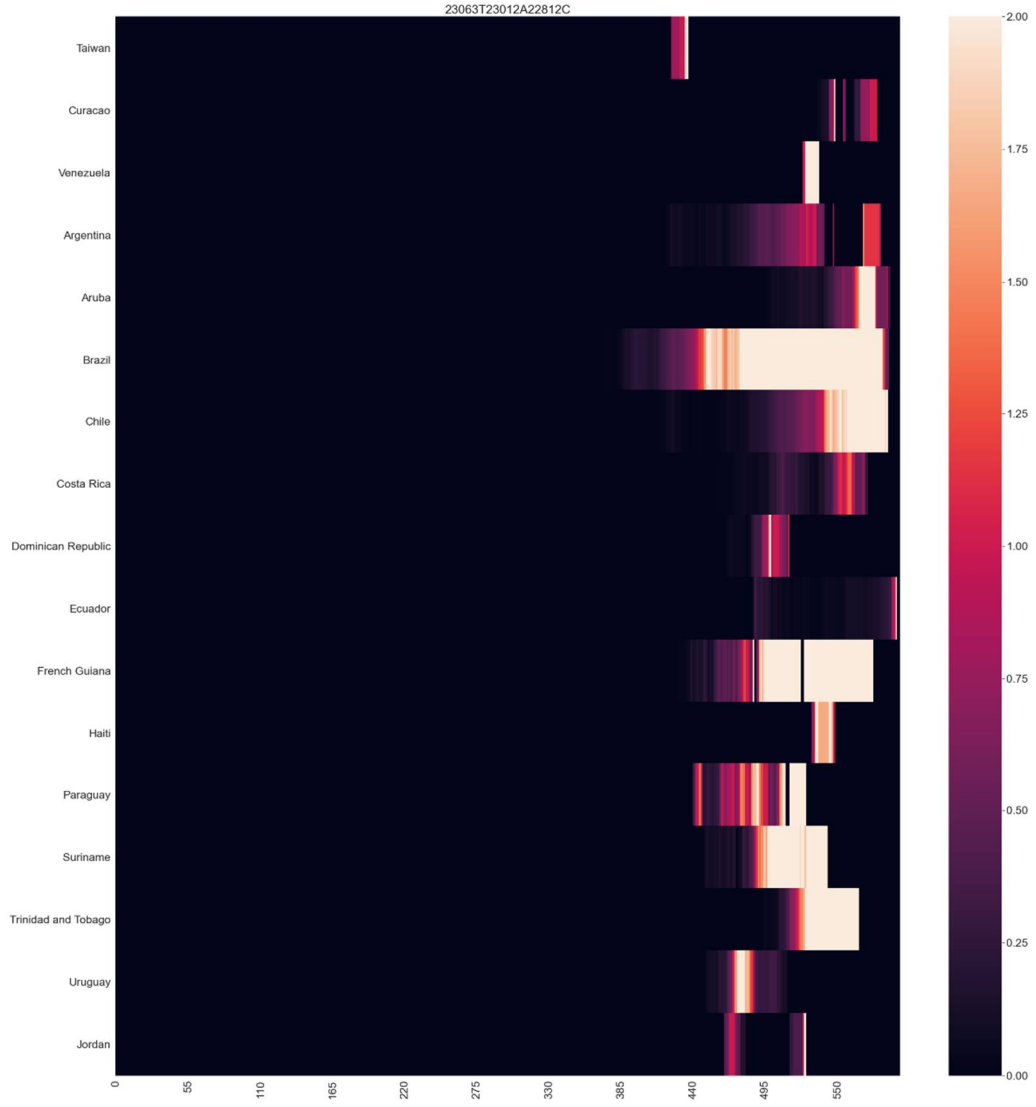
23063T23012A22812C
Taiwan
Curacao
Venezuela
Argentina
Aruba
Brazil
Chile
Costa Rica
Dominican Republic
Ecuador
French Guiana
Haiti
Paraguay
Suriname
Trinidad and Tobago
Uruguay
Jordan
0
55
110
165
220
275
330
385
440
495
550
2.00
1.75
1.50
1.25
1.00
0.75
0.50
0.25
0.00

a)

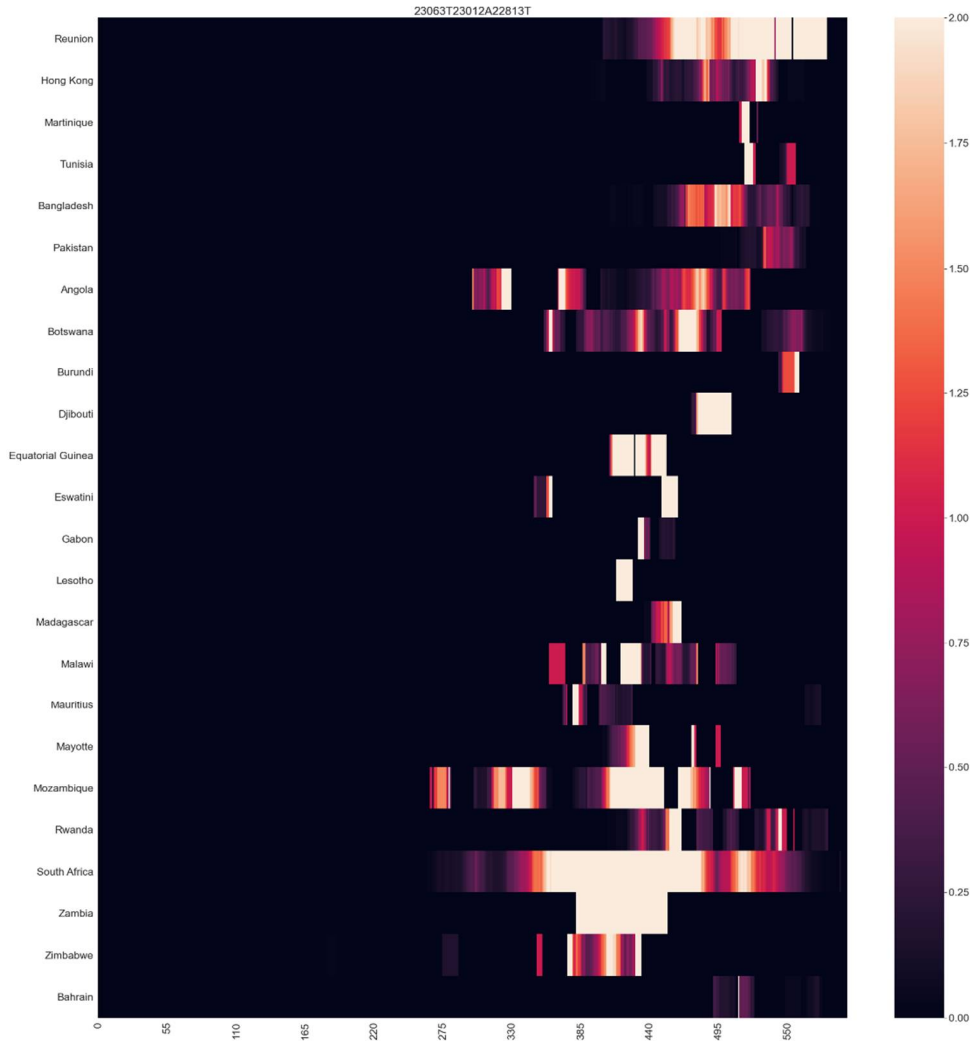

b)

Figure 5. Significant co-occurrences on GISAID of **a)** N501Y, E484K and K417N triple mutations, and **b)** N501Y, E484K and K417T triple mutations, at the virus Receptor Binding Domain (RBD), since the start of the COVID-19 pandemic (31 December 2019). See **Supplementary Table S1** for raw data.